Asymptotic normalization coefficients from the ^{20}Ne(^{3}He, d)^{21}Na reaction and astrophysical factor for ^{20}Ne(p, γ)^{21}Na

A. M. Mukhamedzhanov,[1] P. Bém,[2] V. Burjan,[2] C. A. Gagliardi,[1] B. F. Irgaziev,[3] V. Kroha,[2] J. Novák,[2] Š. Piskoř,[2] E. Šimečková,[2] R. E. Tribble,[1] F. Veselý,[2] and J. Vincour[2]

[1]*Cyclotron Institute, Texas A&M University, College Station, Texas 77843, USA*

[2]*Nuclear Physics Institute of Czech Academy of Sciences, Prague-Řež, Czech Republic*

[3]*Physics Department, National University, Tashkent, Uzbekistan*

(Received 8 August 2005; published 28 March 2006)

The ^{20}Ne(p, γ)^{21}Na reaction rate at stellar energies is dominated by capture to the ground state through the tail of a subthreshold resonance state at an excitation energy of 2425 keV in ^{21}Na. Both resonant and direct capture contribute to the reaction rate while direct captures to other bound states are negligible. The overall normalization of direct capture to the subthreshold state is determined by the asymptotic normalization coefficient (ANC). Simultaneously this ANC determines the proton partial width of the subthreshold resonance state. To determine the ANC, the ^{20}Ne(^{3}He, d)^{21}Na proton transfer reaction has been measured, at an incident energy of 25.83 MeV. Angular distributions for proton transfer to the ground and first three excited states were measured, and ANCs were then extracted from comparison with distorted-wave Born approximation calculations. Using these ANCs, we calculated the astrophysical factor for ^{20}Ne(p, γ)^{21}Na. Our total astrophysical factor is $S(0) = 5900 \pm 1200$ keV b. Our analysis confirms that only nonresonant and resonant captures through the subthreshold state are important.

DOI: 10.1103/PhysRevC.73.035806 PACS number(s): 26.20.+f, 21.10.Jx, 25.55.Hp, 27.30.+t

I. INTRODUCTION

The Ne-Na cycle plays an important role in hydrogen burning in stars with masses larger than that of the sun. The ^{20}Ne(p, γ)^{21}Na reaction, which determines the rate of ^{21}Na stellar production, is the first reaction of the cycle. The nuclei ^{21}Na, ^{21}Ne, ^{22}Na, ^{22}Ne, and ^{23}Na are gradually created during Ne-Na burning. ^{21}Ne nuclei that are produced in the cycle as a result of the ^{21}Na($\beta^+ \nu$)^{21}Ne decay serve as seeds for the neutron generator reaction ^{21}Ne(α, n)^{24}Mg. The ^{20}Ne(p, γ)^{21}Na reaction rate is dominated by s-wave direct capture to the subthreshold state state at $E_x = 2425$ keV in ^{21}Na, which has a spin and parity of $J^\pi = 1/2^+$, and by capture to the ground state through the tail of the subthreshold s-wave resonance at $E_x = 2425$ keV. In stellar environments the ^{20}Ne(p, γ)^{21}Na reaction proceeds at very low energies.

To date, experimental data for the reaction have been measured directly [1] at proton energies of $E_p \geqslant 400$ keV and higher, substantially above the Gamow window. The proton partial width of the subthreshold resonance is determined by the asymptotic normalization coefficient (ANC) for $^{20}\mathrm{Ne} + p \rightarrow {}^{21}\mathrm{Na}(1/2^+,\ 2425\,\mathrm{keV})$ [2]. The same ANC determines the overall normalization of direct capture for ^{20}Ne(p, γ)^{21}Na to this subthreshold state. Because of the very small binding energy of the subthreshold state, 7.1 ± 0.6 keV, and high charge of ^{20}Ne, the direct capture process is totally peripheral at astrophysically relevant energies. This case is ideally suited for the application of the ANC method [3] since the ANC, which is determined by a peripheral proton transfer reaction, allows one to calculate the astrophysical factor for direct capture to the subthreshold state, and, further, it provides a determination of the partial proton width of the subthreshold resonance [2,4].

In previous studies [5,6] we have shown that the (^{3}He, d) proton transfer reaction at incident energies of around 10 MeV/A is a reliable tool to determine ANCs. Here we report a measurement of ANCs for the first four levels in ^{21}Na by the ^{20}Ne(^{3}He,d)^{21}Na reaction.

II. EXPERIMENTAL SETUP AND RESULTS

The experiment was carried out with a momentum-analyzed 25.83 MeV ^{3}He beam (from the U-120M isochronous cyclotron at the Nuclear Physics Institute of the Czech Academy of Sciences) incident upon a neon gas target. The target gas cell contained high-purity isotopic ^{20}Ne (99.99%). The body of the target gas cell had a cylindrical shape with an inner diameter of 104 mm and an inner height of 20 mm. Input and output windows were made from 3.05-μm-thick Havar foils. The working pressure was kept at 195 mbar and was monitored by a gas control system, shown in Fig. 1, which continuously monitored the pressure and temperature of the gas inside the chamber. The control system also was set up to allow for adding gas into the cell in case of a pressure drop that was due to small leaks during the course of the experiment. Reaction products were measured by a pair of $\Delta E - E$ telescopes consisting of 220-μm Si surface barrier detectors and 4-mm-thick Si(Li) detectors. Both telescopes were equipped with a pair of collimating slits of dimension 2 mm $\times$ 3 mm. The near and far slits were 80 and 160 mm, respectively, from the center of the target cell. The effective thickness of the gas target was thus given by the intersection of the solid angle defined by the slits of a telescope and the cylinder corresponding to the circular profile of the incident beam. The effective gas target thickness at different reaction angles for the given geometry was determined by a Monte Carlo simulation. One telescope was fixed at the angle of 19° as a monitor, and the second one was moved during the measurement between laboratory

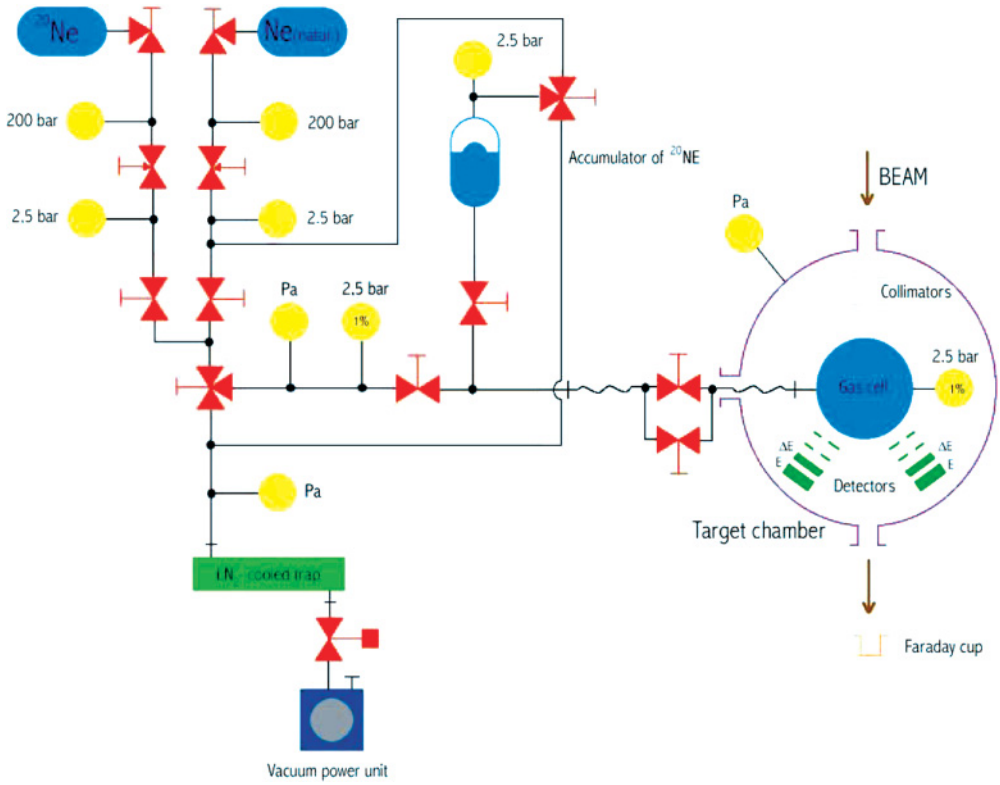

FIG. 1. (Color online) Control system for the neon gas-cell target.

angles of 6.5° and 70°. All measured data, including the charge from the Faraday cup, were collected in an online computer for later analysis. The systematic uncertainty that was due to the effective target thickness and detector solid angle, which are correlated, was estimated to be 8%. An additional uncertainty of 3% was estimated for the charge collection by the Faraday cup. Combining these gives a total systematic uncertainty in the determination of the absolute differential cross section of 8.5% for transitions to all measured states. The total uncertainty, which includes systematic and statistical uncertainties, was estimated to be mostly less than 10% at forward angles with a higher uncertainty for transition to the weakly populated state at $E_x = 1.716$ MeV. Four deuteron groups were identified from the ^{20}Ne(^{3}He, d)^{21}Na reaction below the particle emission threshold of ^{21}Na. A typical deuteron spectrum is shown in Fig. 2. In addition to deuterons that were due to proton transfer to ^{20}Ne, the spectra also contained deuterons from ^{16}O, which likely came from residual water vapor in the cell. No evidence was seen of transitions from ^{14}N that were due to air being in the cell. We also measured spectra from the gas target with natural neon (91% ^{20}Ne, 0.26% ^{21}Ne, and 8.8% ^{22}Ne) to facilitate the identification of deuteron groups. Groups of deuterons corresponding to the excitation of the four bound levels of ^{21}Na (0.0 MeV, $3/2^+$; 0.332 MeV, $5/2^+$; 1.716 MeV, $7/2^+$; and 2.425 MeV, $1/2^+$) can be clearly distinguished in the spectra with isotopic gas. The energy resolution ranged from 100 to 120 keV and was determined by target thickness.

III. OPTICAL-MODEL POTENTIALS AND DISTORTED-WAVE BORN APPROXIMATION CALCULATIONS

The phenomenological optical potential in general form has been used for the analysis of the angular distributions:

$$U(r) = V_c(r) - Vf(x_0) + \left(\frac{\hbar}{m_\pi c}\right)^2 V_{\rm so}(\boldsymbol{\sigma}\cdot\boldsymbol{l})\frac{1}{r}\frac{d}{dr}f(x_{\rm so}) - i\left[Wf(x_w) - 4W_d\frac{d}{dr}f(x_d)\right],$$

where $f(x_i) = (1 + e^{x_i})^{-1}$ and $x_i = (r - r_i A^{1/3})/a_i$ represents the usual Woods-Saxon form factor. V, W, W_d, and $V_{\rm so}$ are the real, imaginary volume, imaginary surface, and spin-orbital potential depths, respectively, with appropriate radius r_i and diffuseness a_i. $V_c(r)$ is the Coulomb potential of a uniformly charged spherical nucleus of a radius $R_c = r_c A^{1/3}$.

The computer code ECIS79 [7] was used to search for optical-model parameters from the elastic-scattering data of ^{3}He on ^{20}Ne. Two sets of optical-model parameters were used as seed parameters in order to include potentials with surface absorption [8] and with volume absorption [9] (see Table I). We did not use seed potentials with spin-orbit coupling. When fitting the optical-model parameters (V, a, W_d, r_d, and a_d or W, r_w, and a_w) we minimized the χ^2 function by using the statistical uncertainties of the elastic-scattering differential cross section. At first, the depths of V and W were looked for while remaining parameters were kept constant. With the new

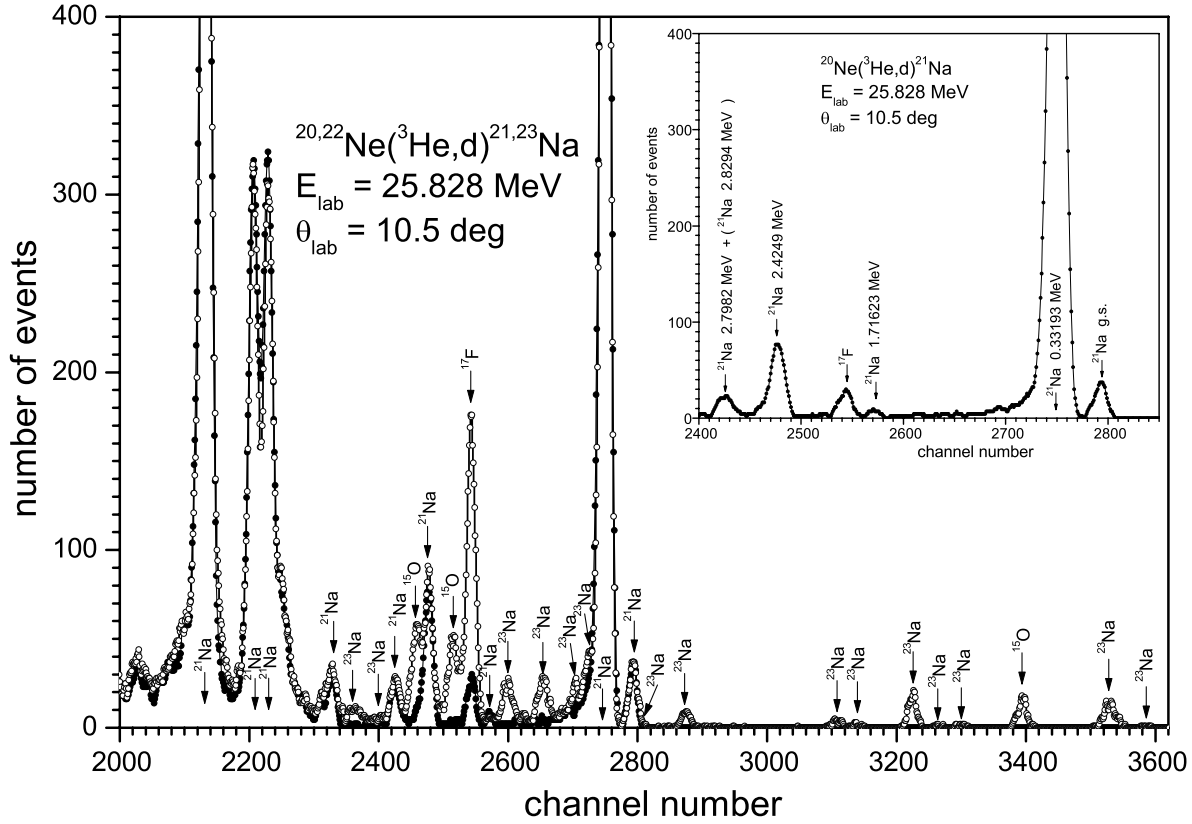

FIG. 2. Deuteron spectrum from the ^{20}Ne(^{3}He,d)^{21}Na reaction at $\theta_{\rm lab} = 10.5^\circ$. The large picture shows the deuteron groups from natural neon gas. The inset shows deuterons from the isotopically pure ^{20}Ne gas.

values of V and W kept constant the procedure was repeated for r_W (r_d) and a_W (a_d) and then for a. Finally, we fit with the new values of five parameters taken as seeds, simultaneously varying all five parameters and also the overall normalization, which changed less than 1%. During the fitting procedure only the statistical uncertainties were taken into account. The resulting optical-model parameters from both seed sets are given in Table I and are denoted as FT (Trost seed calculated from a global formula [8]) and FV (Vernotte family II seed taken from ^{18}O data [9]). We checked the stability of the fits by changing input seed data by 10% to verify that the same optical-model parameters were obtained. Final fits are shown in Fig. 3. Optical-model parameters used for the output channel are given in Table II. They were calculated from the global formulas derived by Daehnick *et al*. [10], set D, and Vernotte *et al*. [11], set V.

Distorted-wave Born approximation (DWBA) calculations for the angular distributions were carried out with the initial-state optical potential parameter sets derived from the fit to elastic-scattering data and the global optical potentials for the exit channel. The energy dependence of the final-state optical potential parameters was taken into account, resulting in the final-state optical potential parameters differing slightly for different final states of ^{21}Na. In Table III the exit channel parameters used for the calculations from Daehnick *et al*. [10] are denoted as sets D0, D1, D2, and D3 for the ground state

TABLE I. Results from the fit of optical-model parameters in the entrance channel ^{3}He + ^{20}Ne. Coulomb radius parameter $r_c = 1.4$ fm.

Potential	V (MeV)	r (fm)	a (fm)	W (MeV)	r_w (fm)	a_w (fm)	W_d (MeV)	r_d (fm)	a_d (fm)
Seed T[a]	112.5	1.15	0.770	—	—	—	20.9	1.286	0.800
Fit FT[b]	107.05	1.15	0.7659	—	—	—	18.92	1.249	0.835
Seed V[c]	173.7	1.15	0.670	13.8	1.849	0.772	—	—	—
Fit FV[d]	177.96	1.15	0.6622	17.39	1.4956	1.0546	—	—	—

[a]Parameters from [8].
[b]Fit of our elastic scattering data.
[c]Parameter set II from [9].
[d]Fit of elastic-scattering data.

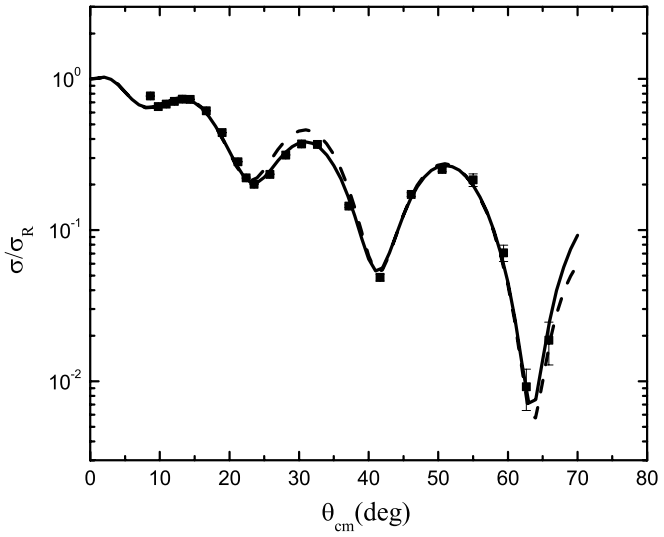

FIG. 3. Final fits to the angular distribution of ^{3}He elastic scattering on ^{20}Ne. The black solid curve is generated by the optical potential set FT and the black dashed curve by T. Potentials are given in Table I.

and first three excited states, respectively, and similarly as V0, V1, V2, and V3 for parameters from Vernotte *et al.* [11]. The angular distributions corresponding to the four states in ^{21}Na calculated with different combinations of the optical-model parameters are given in Fig. 4. The combination FT-V (dot-dashed V red curves s in Fig. 4) provided the best overall fit to the data and consequently was used to determine the ANCs for the different states of ^{21}Na. The angular distribution for the 1.716-MeV state does not correspond to a simple direct transfer. However, coupled-channels calculations usually give similar results as a standard DWBA unless the nuclei are strongly deformed [12].

IV. ASYMPTOTIC NORMALIZATION COEFFICIENTS

For the particle transfer reaction $A(a, b)B$, where $a = b + x$ and $B = A + x$, the DWBA cross section can be written [4] as

$$\frac{d\sigma}{d\Omega} = \left(C^B_{Axl_Bj_B}\right)^2 \left(C^a_{bxl_aj_a}\right)^2 \frac{\tilde{\sigma}^{\rm DW}_{l_Bj_Bl_aj_a}}{b^2_{Axl_Bj_B} b^2_{bxl_aj_a}}, \qquad (1)$$

where $\tilde{\sigma}^{\rm DW}_{l_Bj_Bl_aj_a}$ is the reduced DWBA cross section, $C^a_{bxl_aj_a}$ and $C^B_{Axl_Bj_B}$ are the projectile and final nucleus ANCs, respectively, j_i and l_i are the total and orbital angular momenta respectively, of the transferred particle in nucleus i, and the b's are the single-particle ANCs defining the amplitude of the tail of the radial single-particle bound-state wave functions. The projectile ANC corresponding to the vertex $^3\text{He} \to d + p$ in the channel with $l_{^3\text{He}} = 0$ and $j_{^3\text{He}=1/2}$ is known with very high accuracy: $(C^{^3\text{He}}_{dp21/2})^2 = 3.90 \pm 0.06$ fm^{-1} [13]. This value has been used in the analysis.

The peripheral nature of the transfer reaction can be checked by different methods. A standard approach is to use the cutoff of the radial matrix element of the DWBA amplitude at small radii. The ratio in Eq. (2) offers an equivalent check of the peripheral nature of the transfer process. If the reaction is peripheral the dominant contribution to the reduced DWBA cross section comes from the region in the configuration space where the radial single-particle bound-state wave functions used in the DWBA calculations can be approximated by their

TABLE III. Spectroscopic factors S_{lj} and ANCs from the ^{20}Ne(^{3}He, d)^{21}Na reaction. The first column gives the excitation energy E_x and spin-parity J^π of the state of ^{21}Na; the second column gives the set of the optical potentials in the entrance and exit channels; the third and fourth columns give our results for the spectroscopic factors and ANCs, respectively. The adopted ANC is obtained for the set FT-Vn, $n = 0, 1, 2, 3$. Each adopted ANC is presented with the corresponding uncertainty. A proton binding energy of 7.1 keV has been used for the subthreshold state. The uncertainty for the ANC for the 2.425-MeV state that was due to the experimental uncertainty (600 eV) in the binding energy of this state has not been included here.

State E_x (MeV), (J^π)	Opt. pot.	S_{lj}	C^2_{lj} (fm^{-1})
0.00 $(3/2^+)$	T-D0	0.036538	0.19
	FT-D0	0.034983	0.18
	FV-D0	0.035682	0.19
	FT-V0	0.040885	0.21 ± 0.04
	FV-V0	0.042281	0.22
0.332 $(5/2^+)$	T-D1	0.422925	2.41
	FT-D1	0.409373	2.33
	FV-D1	0.41121	2.34
	FT-V1	0.488267	2.78 ± 0.43
	FV-V1	0.492492	2.80
1.716 $(7/2^+)$	T-D2	0.034353	8.76×10^{-5}
	FT-D2	0.034352	8.76×10^{-5}
	FV-D2	0.032788	8.37×10^{-5}
	FT-V2	0.042937	$(1.10 \pm 0.31) \times 10^{-4}$
	FV-V2	0.041216	1.05×10^{-4}
2.425 $(1/2^+)$	T-D3	0.598278	$6.53311.05 \times 10^{33}$
	FT-D3	0.629058	6.8694×10^{33}
	FV-D3	0.606789	6.6259×10^{33}
	FT-V3	0.562132	$(6.1378 \pm 0.83) \times 10^{33}$
	FV-V3	0.571772	6.2437×10^{33}

TABLE II. Optical-model parameters for outgoing channel $d + ^{21}$Na.

Potential	V (MeV)	r (fm)	a (fm)	W_d (MeV)	r_d (fm)	a_d (fm)	W_{so} (MeV)	r_{so} (fm)	a_{so} (fm)	r_c (fm)	Ref.
D	86.1	1.17	0.7363	12.15	1.325	0.5407	6.7	1.07	0.66	1.3	[10]
V	71.6	1.25	0.7438	13.0	1.25	0.7197	6.0	1.25	0.7338	1.3	[11]

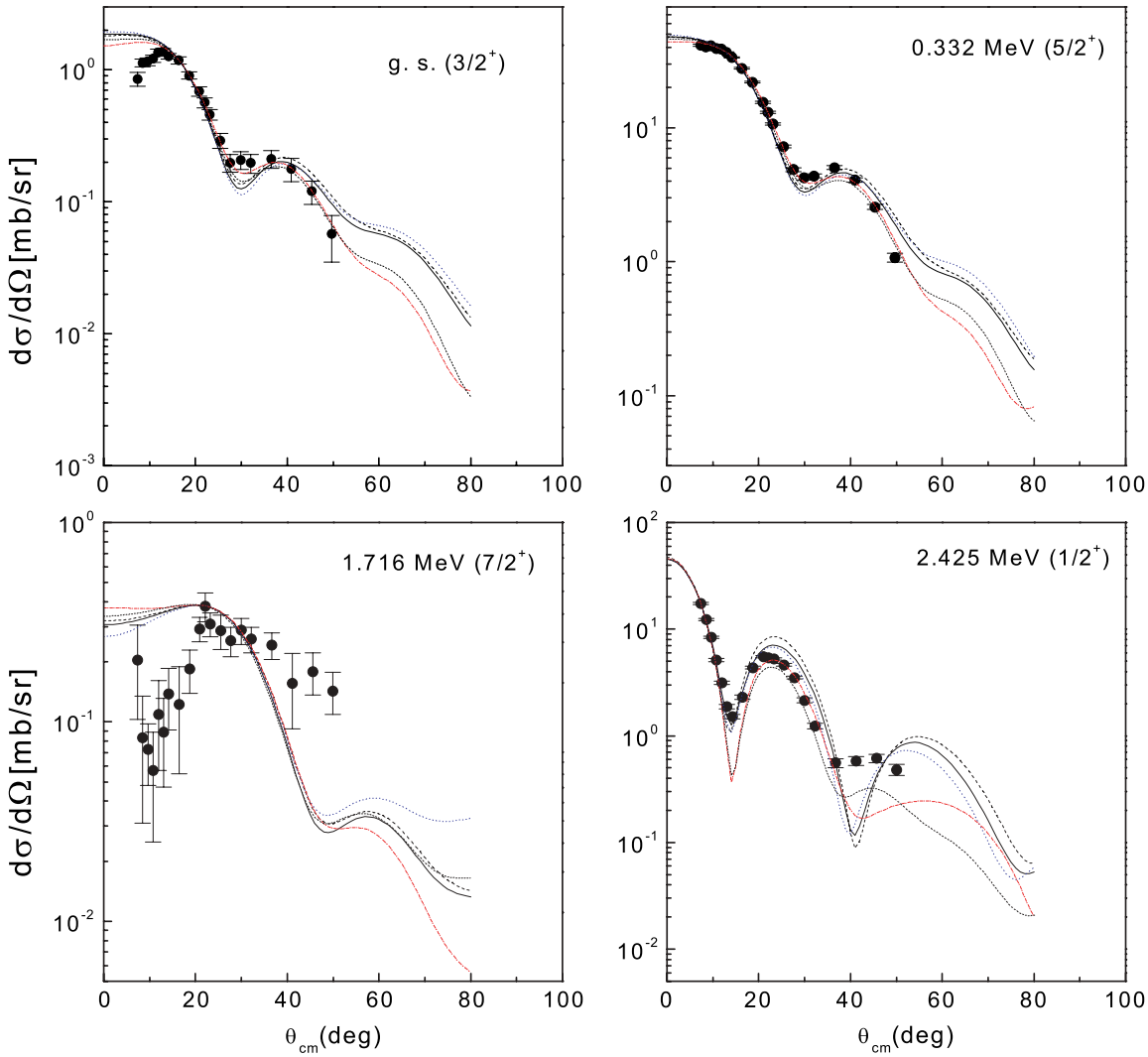

FIG. 4. (Color online) Angular distributions from the ^{20}Ne(^{3}He, d)^{21}Na reaction for transitions to the ground and first three excited states in ^{21}Na. The different sets of optical-model parameters given in Tables I and II are used in the DWBA calculations: black solid curve, T-D; black dashed curve, FT-D; blue dotted curve, FV-D; red dash-dotted curve, - FT-V; black dotted curve, FV-V.

tails, i.e., $\tilde{\sigma}^{\mathrm{DW(max)}}_{l_B j_B l_a j_a} \sim b^2_{Axl_B j_B} b^2_{bxl_a j_a}$, and the ratio

$$R\left(b_{Axl_B j_B}, b_{bxl_a j_a}\right) = \frac{\tilde{\sigma}^{\mathrm{DW(max)}}_{l_B j_B l_a j_a}}{b^2_{Axl_B j_B} b^2_{bxl_a j_a}}, \qquad (2)$$

where $\tilde{\sigma}^{\mathrm{DW(max)}}$ is the reduced DWBA differential cross section calculated at the main (first) maximum of the angular distribution, is independent of the single-particle ANCs $b_{Axl_B j_B}$ and $b_{bxl_a j_a}$ [4]. We checked the dependence of R on the single-particle ANC, $b_{Axl_B j_B}$, for the bound-state wave function $^{20}\mathrm{Ne} + p$. (For simplicity in what follows we drop the subscripts in the single-particle ANC b.) In Eq. (2) the reduced DWBA differential cross section was calculated at the main maximum of the angular distribution, which is the most forward—pronounced—peak in the transfer reaction and typically occurs at or near 0°. In the vicinity of the main maximum, the transfer reaction is the most peripheral, and a simple particle transfer mechanism (stripping) described by the DWBA gives the dominant contribution. We calculated $R(b)$ by using the combination of the optical potential sets FT-V in Tables I and II. One can achieve variation of the single-particle ANC by changing the geometrical parameters, radius r_0 and diffuseness a, of the Woods-Saxon bound-state potential, since the single-particle ANC depends on these parameters. The radius r_0 was changed from 1.05 to 1.7 fm at fixed diffuseness of $a = 0.65$ fm. This variation of r_0 for the subthreshold state changes b by 40%. The change for more tightly bound states is significantly higher. The calculations of $R(b)$ have been done for transitions to the ground state, first excited state $E_x = 0.332$ MeV, and the subthreshold state $E_x = 2.425$ MeV. The results shown in Fig. 5 demonstrate that the proton transfer reaction is peripheral, especially for the most important transition to the 2.425-MeV state, where $R(b)$ is practically flat.

The ANCs for the ground and three excited bound states of ^{21}Na resulting from the analysis are given in Table III. From

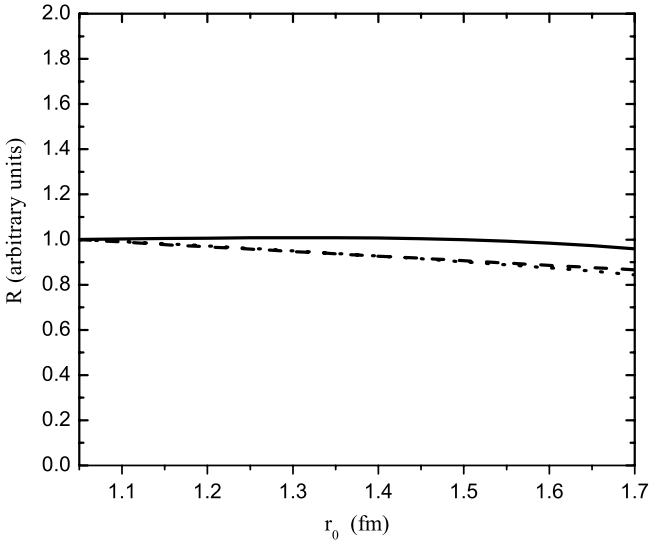

FIG. 5. The ratio R for three transitions from the ^{20}Ne(^{3}He, d)^{21}Na reaction. The solid line and dashed and dotted curves are for the transitions to the subthreshold state, the ground state, and the first excited state, respectively.

Table III we can infer the uncertainty of the ANCs for each state because of the ambiguity of the optical potentials. If we also take into account the uncertainty of the absolute cross section, we find that the total uncertainties of the ANCs range from 14% (2.425-MeV state) to 28% (1.716-MeV state). The ANC for the subthreshold state is especially important for nuclear astrophysics. The binding energy of this state is $\varepsilon = 7.1 \pm 0.6$ keV, i.e., it is typical of an atomic rather than a nuclear scale. A variation of the binding energy by just a few hundred electron volts changes the ANC by orders of magnitude. In Table IV the dependence of the extracted ANC on the binding energy for the subthreshold state is presented.

Since the reaction chosen here is peripheral it is not suitable for determination of the spectroscopic factor. There is a simple physical reason: The spectroscopic factor, by definition, is the square norm of the overlap function of the bound-state wave functions of A, x, and B and the dominant contribution to the norm comes from the nuclear interior. The ANC determined from the peripheral reaction is related to the spectroscopic factor by

$$S_{lj} = \frac{C_{lj}^2}{b_{lj}^2}. \tag{3}$$

The single-particle ANC is determined by the parameters of the single-particle bound-state potential, and hence the same is true for the extracted spectroscopic factor. In Table III we present the spectroscopic factors we calculated by using b_{lj} generated by the standard values of the geometrical parameters of the proton bound state, radius $r_0 = 1.25$ fm, diffuseness $a = 0.65$ fm, and the Coulomb radius parameter $r_C = 1.4$ fm for comparison. Our spectroscopic factors are significantly lower than those determined in Ref. [1], since Rolfs *et al.* used a rectangular well in their analysis. The rectangular well corresponds to the limit of the Woods-Saxon potential with diffuseness $a \to 0$. This just demonstrates that it is meaningless to compare the spectroscopic factors corresponding to the different parameters of the bound-state potentials [14].

TABLE IV. ANCs for the subthreshold state at $E_x = 2.425$ MeV determined from the ^{20}Ne(^{3}He, d)^{21}Na reaction for different proton separation energies. The optical potentials used to calculate the DWBA cross section are given in the first column.

Opt. pot.	6.6 keV ($\times 10^{35}$)	6.8 keV ($\times 10^{34}$)	7.1 keV ($\times 10^{33}$)	7.3 keV ($\times 10^{33}$)	7.5 keV ($\times 10^{32}$)
T-D3	3.5615	6.8282	6.5331	1.4602	3.6264
FT-D3	3.7448	7.1797	6.8694	1.5353	3.8130
FV-D3	3.6121	6.9252	6.6259	1.4809	3.6779
FT-V3	3.3460	6.4151	6.1378	1.3718	3.4069
FV-V3	3.4037	6.5258	6.2437	1.3955	3.4657

V. ASTROPHYSICAL FACTOR FOR ^{20}Ne(p, γ)^{21}Na

As we have noted, the subthreshold s-wave bound state at $E_x = 2.425$ MeV plays a crucial role in the determination of the astrophysical $S(0)$ factor for ^{20}Ne(p, γ)^{21}Na. Because of the "ultrasmall" binding energy of the subthreshold state and the low energies important for stellar capture, direct radiative capture to the subthreshold state is extremely peripheral. Consequently the overall normalization of the astrophysical factor for direct radiative capture to the subthreshold state at stellar energies is determined entirely by its ANC [5]. To calculate the S factor we have used the R-matrix approach in which the normalization of the external nonresonant capture amplitude is governed by the ANC of the final bound state [15,16]. At energies at which experimental data exist, direct capture through the subthreshold state dominates the S factor. The direct radiative capture process to the subthreshold state is so peripheral that a variation of the channel radius by 60% (from 5 to 8 fm) changes the astrophysical factor by only 2.0% at a proton energy of 250 keV. Hence, a comparison of the calculated S factor to the data [1] is a test of the accuracy of the ANC determined from the transfer reaction. This comparison is shown in Fig. 6.

To obtain a 1% calculational accuracy for the radial matrix element for direct radiative capture to the subthreshod state, the upper integration limit was extended to 1600 fm. For the calculation we use the square of the ANC $C_{lj}^2 = 7.0 \times 10^{33}$ fm^{-1}, which is the upper limit of the adopted ANC for the subthreshold $1/2^+$ state (see Table III) and provides the best fit to the experimental data. The calculated S factor for direct capture is $S(0) = 68.30 \pm 9.30$ keV b. The uncertainty is entirely due to the uncertainty in the ANC determined from the transfer reaction. Our calculated value agrees very well with the experimental data from Ref. [1] for $E > 307$ keV, where E is the relative kinetic energy of the proton and ^{20}Ne. We note that the calculated astrophysical factor does not depend on the uncertainty in the binding energy. In the R-matrix approach, the nonresonant S factor contains the

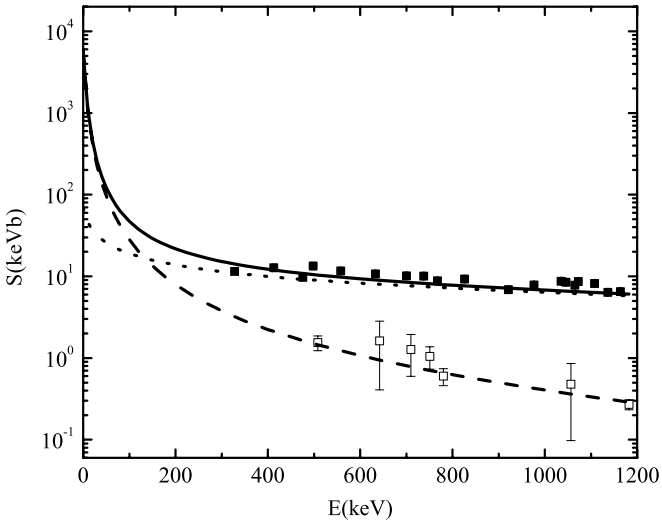

FIG. 6. The ^{20}Ne$(p,\gamma)^{21}$Na astrophysical S factor. The solid squares and dotted curve are the experimental data points [1] and our result for direct capture to the subthreshold state, respectively; the open squares and dashed curve are the experimental data points [1] and our result for capture to the ground state through the subthreshold resonance, respectively; the solid curve is our total astrophysical factor.

term $C_{lj}^2\, W_{-\eta,l+1/2}^2(2\,r_{\rm ch})$, which is not sensitive to the binding energy variation; a strong variation of the ANC C_{lj}^2 is compensated for by a corresponding variation of the hypergeometric function $W_{-\eta,l+1/2}^2(2\,r_{\rm ch})$, where η is the Coulomb parameter of the bound state, l is the orbital angular momentum of the proton bound state in ^{21}Na, and $r_{\rm ch}$ is the channel radius used in the R-matrix calculation. We adopted $r_{\rm ch} = 5$ fm, as in [1] but, as noted above, the direct radiative capture calculation is not sensitive to the channel radius. Although our result for $S(E)$ agrees very well with the data from [1] at higher energies, our $S(0)$ value is significantly higher than the $S(0) = 40.00 \pm 4.40$ keV b obtained in [1]. We suspect that the low value for $S(0)$ in [1] is the result of an improper extrapolation to zero energy. In particular, $S(0)$ is very sensitive to the upper limit of the integral in the radial matrix element. For example, an upper limit of $R = 700$ fm gives $S(0) = 39.55$ keV b rather than $S(0) = 68.30$ keV b for $R = 1600$ fm. However for $E > 30$ keV, $S(E)$ becomes insensitive to the upper limit of R for $R > 500$ fm.

Capture to the ground state, $J^\pi = 3/2^+$, is dominated by resonance capture through the subthreshold state. Direct capture to the ground state is negligibly small compared with the resonance capture component, and it does not interfere with the resonance transition because the orbital angular momentum in the initial state for the resonance capture is $l_i = 0$ while for the direct $E1$ capture it is $l_i = 1$. Our calculated astrophysical factor for the $E1$ direct capture to the ground state is $S(E) < 0.048$ keV b for $E < 0.5$ MeV and $S(0) = 0.0463$ keV b. These values agree with estimates of the upper limit for direct capture to the ground state in Ref. [1]. To calculate the astrophysical factor for resonance capture to the ground state through the subthreshold state, we need to know the proton partial width and the radiative width for the decay to the ground state. The proton partial width is determined by the ANC for the subthreshold resonance [2] by

$$\Gamma_p = P_l\, \frac{W_{-\eta,l+1/2}^2(2\,r_{\rm ch})}{\mu\, r_{\rm ch}}\, |C|^2. \qquad (4)$$

Here, P_l is the penetrability factor for the lth partial wave corresponding to the subthreshold resonance, C is the ANC of the subthreshold state, and μ is the reduced mass of the scattering particles. Note that the partial width Γ_p is insensitive to the variation of the proton binding energy of the subthreshold state because the product $|C|^2\, W_{-\eta,l+1/2}^2(2\,r_{\rm ch})$ is stable. For analysis we use the higher value of the ANC for the proton binding energy of the subthreshold state $\varepsilon = 7.10$ keV from Table III. The ratio of our proton partial width calculated at $E = 1$ keV to the corresponding observable width calculated with parameters presented in [1] is 0.88. Correspondingly the ratio of our radiative width at $E = 1$ keV to that reported in Ref. [1] is 1/0.88.

The radiative width has been used as a scaling parameter to normalize the calculated astrophysical factor to the experimental data [1]. The best fit to the experimental data is obtained for the observable $\Gamma_\gamma(0) = 0.16 \pm 0.04$ eV. This value is close to the observed radiative width $\Gamma_\gamma(0) = 0.14 \pm 0.03$ reported in Ref. [1], and it is significantly below the the lower limit of $\Gamma_\gamma(0) > 0.33$ determined in Ref. [17] by use of the Doppler shift method. Since the orbital angular momentum of the ground state is $l_f = 2$, resonant capture through the subthreshold state can have $M1$ and $E2$ contributions. Formal estimates of the astrophysical factor for both transitions lead to very similar results. As in Ref. [1] we assume that the resonance transition is $M1$. The experimental and calculated $S(E)$ factors for the resonance transition to the ground state are displayed in Fig. 6. Since we determine the astrophysical factor by fitting to the experimental data by using the radiative width as a scaling factor, the uncertainty in the astrophysical factor for the resonance transition is determined by the experimental uncertainty. We find that the astrophysical factor for resonant capture to the ground state is $S(0) = 5870.0 \pm 1200$ keV b, which is higher than the value $S(0) = 3500$ keV b found in Ref. [1]. The calculations were done for a channel radius of $r_{\rm ch} = 5$ fm. Changing $r_{\rm ch}$ by 20% does not affect the $S(0)$ factor. Our $S(0)$ factor exceeds that presented in [1] because of a more accurate extrapolation down to zero energy used here. Note that the uncertainty of 1200 keV b found in the present work represents the range of values for the radiative width Γ_γ that is consistent with the statistical uncertainties for the data in Ref. [1]. Unfortunately no systematic uncertainty for $S(0)$ is presented in Ref. [1]. There are two narrow resonances above threshold, $1/2^-$ at 366 keV, with $\Gamma = 3.8$ meV, and $9/2^+$ at 397 keV, that were observed. Both resonances have proton widths of the order of milli-electron-volts and do not affect the S factor at low energies. We did not include them in the calculation nor did we take into account higher-lying resonances since their contribution to the $S(E)$ factor at astrophysically relevant energies is also negligible [1]. In Fig. 6 we compare our results and the experimental results for the total $S(E)$ factors. Our calculated total $S(E)$ is given by the sum of the direct capture contribution to the subthreshold state

and the contribution for capture to the ground state through the subthreshold resonance and $S(0) = 5900 \pm 1200$ keV b.

VI. SUMMARY AND CONCLUSION

ANCs were determined for low-lying states of ^{21}Na from the angular distributions measured in the ^{20}Ne(^{3}He, d)^{21}Na reaction. The ANCs were used to calculate the astrophysical S factor for the (p, γ) radiative direct capture reaction on ^{20}Ne at low energies. The only significant contribution to the astrophysical factor comes from the subthreshold state at $E_x = 2.425$ MeV. Consequently we present the astrophysical factors only for direct capture to the subthreshold state and capture to the ground state through the subthreshold state. Our ANC for the subthreshold state allows us to reproduce direct capture experimental data to the subthreshold state. However, the astrophysical factor for direct capture to the second excited state at $E_x = 0.332$ MeV calculated from the ANC determined from the transfer reaction is $S(0) = 1.4$ keV b, which does not agree well with the experimental value of 4.0 keV b [1]. We do not know the reason for this difference, but the first excited state produces a negligible contribution to the reaction rate. It is also not clear why there is a significant difference between the radiative width for the subthreshold resonance state reported in Ref. [17] and that obtained from fitting of the experimental data in Ref. [1]. We believe new measurements would be very useful in clearing up these problems.

ACKNOWLEDGMENTS

Consultations on the Monte Carlo method with A. Špalek are appreciated. This work was supported by the U.S. Department of Energy under grant no. DE-FG02-93ER40773, the U.S. National Science Foundation under grant no. INT-9909787 and grant no. PHY-0140343, ME 385(2000) and ME 643(2003) projects NSF and MSMT, CR, project K1048102, and grant no. 202/05/0302 of the Grant Agency of the Czech Republic, and by the Robert A. Welch Foundation.

[1] C. Rolfs, W. S. Rodney, M. S. Shapiro, and H. Winkler, Nucl. Phys. **A241**, 460 (1975).
[2] A. M. Mukhamedzhanov and R. E. Tribble, Phys. Rev. C **59**, 3418 (1999).
[3] H. M. Xu, C. A. Gagliardi, R. E. Tribble, A. M. Mukhamedzhanov, and N. K. Timofeyuk, Phys. Rev. Lett. **73**, 2027 (1994).
[4] A. M. Mukhamedzhanov, H. L. Clark, C. A. Gagliardi, Y.-W. Lui, L. Trache, R. E. Tribble, H. M. Xu, X. G. Zhou, V. Burjan, J. Cejpek, V. Kroha, and F. Carstoiu, Phys. Rev. C **56**, 1302 (1997).
[5] C. A. Gagliardi, R. E. Tribble, A. Azhari, H. L. Clark, Y.-W. Lui, A. M. Mukhamedzhanov, A. Sattarov, L. Trache, V. Burjan, J. Cejpek, V. Kroha, Š. Piskoř, and J. Vincour, Phys. Rev. C **59**, 1149 (1999).
[6] A. M. Mukhamedzhanov, P. Bém, B. A. Brown, V. Burjan, C. A. Gagliardi, V. Kroha, J. Novák, F. M. Nunes, Š. Piskoř, F. Pirlepesov, E. Šimečkova, R. E. Tribble, and J. Vincour, Phys. Rev. C **67**, 065804 (2003).
[7] J. Raynal, code ECIS79 (unpublished), (see http://www.fr/abs/html/nea-850.html).
[8] H. J. Trost, P. Lezoch, and U. Strohbusch, Nucl. Phys. **A462**, 333 (1987).
[9] J. Vernotte, G. Berrier-Ronsin, J. Kalifa, and R. Tamisier, Nucl. Phys. **A390**, 285 (1982).
[10] W. W. Daehnick, J. D. Childs, and Z. Vrcelj, Phys. Rev. C **21**, 2253 (1980).
[11] J. Vernotte, G. Berrier-Ronsin, J. Kalifa, R. Tamisier, and B. H. Wildenthal, Nucl. Phys. **A571**, 1 (1994).
[12] F. M. Nunes and A. M. Mukhamedzhanov, Phys. Rev. C **64**, 062801(R) (2001).
[13] A. M. Mukhamedzhanov, R. E. Tribble, and N. K. Timofeyuk, Phys. Rev. C **51**, 3472 (1995).
[14] A. M. Mukhamedzhanov, C. A. Gagliardi, and R. E. Tribble, Phys. Rev. C **63**, 024612 (2001).
[15] F. C. Barker and T. Kajino, Aust. J. Phys. **44**, 369 (1991).
[16] X. Tang, A. Azhari, C. A. Gagliardi, A. M. Mukhamedzhanov, F. Pirlepesov, L. Trache, R. E. Tribble, V. Burjan, V. Kroha, and F. Carstoiu, Phys. Rev. C **67**, 015804 (2003).
[17] J. Dubois, H. Odelius, and S. O. Berglund, Phys. Scr. **5**, 16 (1972).